



Article

One-Pot Synthesis of Acidic Mesoporous Activated Carbon Obtained from Yerba Mate Twigs as Suitable Catalyst for the Production of Levulinic Ester Biofuel Additives

John J. Alvear-Daza ¹ , Alexis Sosa ¹, Diego M. Ruiz ², Gustavo A. Pasquale ², Julián A. Rengifo-Herrera ¹, Gustavo P. Romanelli ^{2,*} and Luis R. Pizzio ^{1,*} 

- ¹ Centro de Investigación y Desarrollo en Ciencias Aplicadas “Dr. J.J. Ronco” (CINDECA), Departamento de Química, Facultad de Ciencias Exactas, Universidad Nacional de La Plata-Centro Científico Tecnológico La Plata, Consejo Nacional de Investigaciones Científicas y Técnicas, 47 No. 257, La Plata B1900AJK, Argentina; johalvear@quimica.unlp.edu.ar (J.J.A.-D.); asosa@quimica.unlp.edu.ar (A.S.); julianregifo@quimica.unlp.edu.ar (J.A.R.-H.)
- ² Centro de Investigación en Sanidad Vegetal (CISaV)/Cátedra de Química Orgánica, Facultad de Ciencias Agrarias y Forestales, Universidad Nacional de La Plata, Calles 60 y 119 s/n, La Plata B1904AAN, Argentina; gustavo.pasquale@agro.unlp.edu.ar (G.A.P.)
- * Correspondence: gpr@quimica.unlp.edu.ar (G.P.R.); lrpizzio@quimica.unlp.edu.ar (L.R.P.)

Abstract: A series of activated carbons (YMBC) obtained from yerba mate twig residue (YMT) were prepared by chemical (H_3PO_4) and thermal activation. Five materials were synthesized, varying the carbonization temperature (400–600 °C under N_2 atmosphere) and H_3PO_4 :YMT ratio (60–80 wt%). They were physicochemically and texturally characterized by SEM-EDX, BET, FT-IR, and ^{31}P MAS-NMR. Potentiometric titration with the n-butylamine technique was used to evaluate their acidic properties. The materials exhibited a high specific surface area ($572 \text{ m}^2 \text{ g}^{-1} < S_{\text{BET}} < 1031 \text{ m}^2 \text{ g}^{-1}$) and mesoporosity ($67\% < S_{\text{meso}}/S_{\text{BET}} < 93\%$). The results showed that the acid strength and the number of acid sites increased with the H_3PO_4 :YMT ratio and decreased with the calcination temperature increment. The FT-IR and ^{31}P characterization revealed the presence of $\text{H}_{n+2}\text{P}_n\text{O}_{3n+1}$ species firmly (via P-O-C linkages) and loosely attached (by electrostatic interaction). The latter were successfully removed by refluxing the material in water or n-propanol. The optimal reaction conditions were applied to the synthesis of other levulinic acid esters using YMBC-500-70_{NP} as a catalyst. Furthermore, the effective separation of the product combined with the use of a recyclable catalyst resulted in a clean and environmentally friendly strategy for the synthesis of alkyl levulinates, bioproducts of relevance to the biorefinery industry, which can be applied as fragrances, flavoring agents, as well as fuel additives.

Keywords: esterification; levulinic acid; levulinate ester; mesoporous activated carbon; yerba mate twigs



Citation: Alvear-Daza, J.J.; Sosa, A.; Ruiz, D.M.; Pasquale, G.A.; Rengifo-Herrera, J.A.; Romanelli, G.P.; Pizzio, L.R. One-Pot Synthesis of Acidic Mesoporous Activated Carbon Obtained from Yerba Mate Twigs as Suitable Catalyst for the Production of Levulinic Ester Biofuel Additives. *Catalysts* **2024**, *14*, 522. <https://doi.org/10.3390/catal14080522>

Academic Editor: Xiaofeng Wang

Received: 26 June 2024

Revised: 2 August 2024

Accepted: 8 August 2024

Published: 13 August 2024



Copyright: © 2024 by the authors. Licensee MDPI, Basel, Switzerland. This article is an open access article distributed under the terms and conditions of the Creative Commons Attribution (CC BY) license (<https://creativecommons.org/licenses/by/4.0/>).

1. Introduction

Levulinic acid (LA) is a biomass-derived compound platform containing carboxylic acid and a ketone group with many substituents. Among the large number of derived substances are levulinic esters [1–3], which are widely used as solvents in the flavoring and polymer industry. In particular, ethyl levulinate is interesting because it can be used as a green solvent [4] and fuel additive [5] because of its higher engine performance, longer life, and lower CO and NO_x emissions [6,7].

These esters are typically produced by esterification reactions using homogeneous catalysts such as hydrochloric, sulphuric, and phosphoric acids, which provide high ester yields in short periods of time. However, in these homogeneous catalytic reactions, the acids are not recyclable; they need to be neutralized using large amounts of base and generate salts that need to be properly disposed of. In recent years, the search for environmentally

benign and sustainable chemical processes has attracted much attention. Therefore, one of the proposed alternatives is to use an acid catalyst that operates in a heterogeneous form, where the catalyst can be easily separated and reused, to develop an economically and environmentally strategy [8–14].

Various solid acid catalysts have been tested to this end; zeolites [15], acid resin [13,16], silica modified with a $-\text{SO}_3\text{H}$ group [17], sulfonated carbon [18], and sulfonated ZrO_2 [19] have been investigated as potential catalysts to achieve levulinic acid esterification. For a more comprehensive overview of catalysts reported in the literature for the esterification of levulinic acid with alcohol, the following references can be consulted [20–24]. The solid catalysts listed in the literature for the esterification of levulinic acid with ethanol were mainly prepared from more expensive nonrenewable materials using more than one synthesis step. Only a few were obtained from renewable materials (D-glucose, cellulose powder, and corn stalks) but using more than one synthesis step (see Table S1 in the Supplementary Materials).

Mesoporous-carbon-based acid catalysts have been used as highly active, selective, and reusable solid catalysts for the esterification of different substrates, including succinic, fumaric, levulinic, and itaconic acids [10,18,25]. They are usually synthesized using glucose, sucrose, cellulose, starch, and resorcinol–formaldehyde resins as a carbon source. Sulfonic groups were incorporated using sulfuric, p-toluenesulfonic, benzene sulfonic, and chlorosulfonic acid treatments. On the other hand, we reported the synthesis of mesoporous activated carbon by chemical (H_3PO_4) and thermal ($600\text{ }^\circ\text{C}$) activation of sunflower seed shells (an agro-industrial waste generated in great amounts by the sunflower oil industry), and its sulfonation (by chlorosulfonic acid treatment) [26]. This procedure allowed us to obtain very active and selective acid catalysts for the esterification reaction of itaconic acid with ethanol. To explore the potential of other local agro-industrial wastes to synthesize mesoporous carbon, we focus our attention on yerba mate (*Ilex paraguariensis*) twigs.

For the manufacture of yerba mate, the whole branches of *Ilex paraguariensis* Saint Hilaire tree are processed. According to the Argentine food code, the elaborated yerba mate (massively consumed in Argentina, Brazil, Paraguay, and Uruguay to prepare a popular herbal infusion named “mate”) should contain at least 65% leaves (dried, broken or pulverized) and at most 35% twigs. According to the National Yerba Mate Institute, in 2023 in Argentina 774,167 tons were processed to obtain 325,121 tons of elaborated yerba mate. As a result, a huge volume of twigs is disposed of, thus constituting an attractive biomass waste for its conversion into activated carbon. Recently, ultramicroporous and micro-mesoporous activated carbon were synthesized using yerba mate waste as a lignocellulosic source and KOH as a chemical activating agent to be used for greenhouse gas adsorption and supercapacitors, respectively [27–29].

To the best of our knowledge, this is the first study that reports the one-pot synthesis of acidic mesoporous activated carbon from yerba mate twigs to be used as a catalyst in heterogeneous levulinic acid esterification. The effects of several experimental activated carbon syntheses (calcination temperature and chemical activating agent/YMT ratios) and levulinic acid esterification reaction conditions (time, temperature, catalyst amount, etc.) were analyzed in order to develop a clean and environmentally friendly strategy for the synthesis of levulinic acid esters.

2. Results and Discussion

Figure 1a shows the effect of T (carbonization temperature, $^\circ\text{C}$) and H_3PO_4 :YMT ratio (wt%) on the development of specific surface area. The RSM reveals that the specific surface area values can be enhanced when a temperature $\sim 600\text{ }^\circ\text{C}$ and H_3PO_4 :YMT ratio equal to 80 wt% are employed to synthesize YMBC. In these conditions (Tables 1 and 2), YMBC with $S_{\text{BET}} = 1031\text{ m}^2\text{ g}^{-1}$ and $D_p = 2.3\text{ nm}$ (the highest S_{BET} and the lower pore diameter, respectively) was obtained.

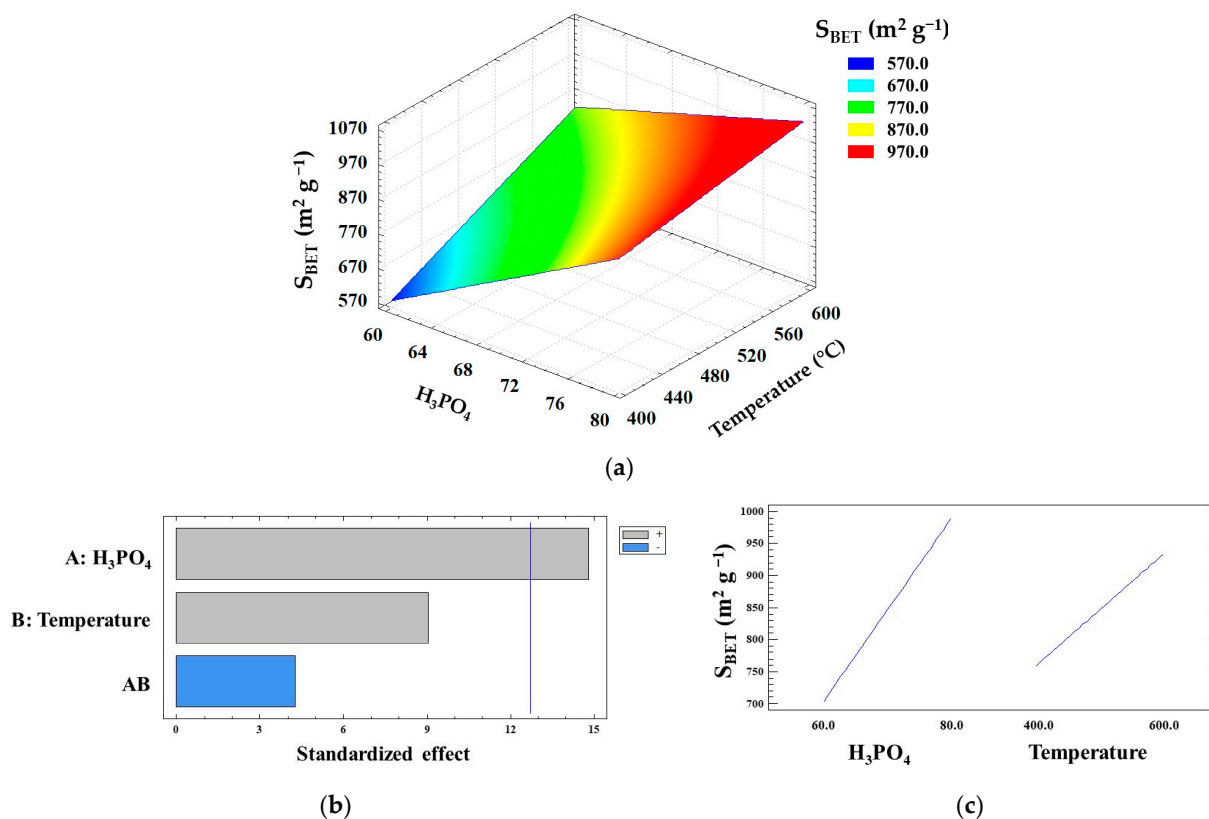


Figure 1. Development of S_{BET} following 2^2 factorial design (a), RMS of S_{BET} , Pareto drawing (b), and activating factor interaction drawing (c).

Table 1. Experimental design of factorial 2^2 -type for the synthesis of YMBC from yerba mate twigs.

Factors	Levels		
	Low (−)	Central Point (0)	High (+)
x_1 : H_3PO_4 :YMT ratio (wt%)	60	70	80
x_2 : carbonization temperature (°C)	400	500	600
Run	Sample name	x_1	x_2
1	YMBC-400-60	60	400
2	YMBC-400-80	80	400
3	YMBC-600-60	60	600
4	YMBC-600-80	80	600
5	YMBC-500-70	70	500

Table 2. Main textural properties of YMBC samples.

Experimental Design				Textural Properties		
Run	Sample Name	Level		S_{BET}	S_{meso}	Dp
		A Factor	B Factor	m ² g ⁻¹	m ² g ⁻¹	nm
1	YMBC-400-60	−	−	572	485	4.2
2	YMBC-400-80	+	−	828	769	3.8
3	YMBC-600-60	−	+	939	870	3.2
4	YMBC-600-80	+	+	1031	686	2.3
5	YMBC-500-70	0	0	864	707	3.6

The ANOVA (Table 3) of the experimental design for YMBC preparation displays that the effect of H_3PO_4 concentration (A factor) has a p -value < 0.05 (95% confidence level). The

H₃PO₄ concentration has a greater significance, as is revealed in Figure 1b. Figure 1c shows that the increment of S_{BET} is more significant when the H₃PO₄:YMT ratio increases at the highest carbonization temperature. The ANOVA reveals that R^2 (the square of deviation) explains 99% of the S_{BET} experimental value regression correlation (the response variable), and the p -value (<0.05) represents a statistically significant effect for the H₃PO₄:YMT ratio, as shown in Figure 1b.

Table 3. Summary of analysis of variance (ANOVA) for the response surface.

Factors	Sum of Squares	F-Value	p -Value
A:	81,225.0	219.6	0.0429
B:	30,276.0	81.8	0.0701
AB	6724.0	18.2	0.1466
Total error	369.8		
R^2	99.6		
Standard error	19.23		
Absolute error	6.8		
Durbin–Watson	2.5		

SEM micrographs of YMT and YMBC (see Figure S1 in the Supplementary Materials) show the characteristic wide tubular channels of the vegetal structure. This structure remained unmodified by the activation treatment. The EDX results show the presence of phosphorus, oxygen, and silicon in the carbon matrix. The presence of phosphorus is due to the treatment with phosphoric acid. The DRX diffractogram of the YMBC-500-70 sample (see Figure S2 in the Supplementary Materials) shows two diffraction planes associated with the carbon plane (002), indicating a parallel orientation and azimuthal orientation of the partially carbonized aromatic sheets, and the carbon crystalline plane (100), associated with carbonized planes of condensed aromatics, respectively [30]. No significant differences were present in the DRX diffractograms of the other materials.

The N₂ adsorption–desorption isotherms of YMBC materials are shown in Figure 2a. According to IUPAC, they can be classified as type IV, characteristic of mainly mesoporous materials, with an H4 hysteresis loop [31]. The YMBC-600-80 sample displays the highest S_{BET} value (1031 m² g^{−1}); however, the percentage of the S_{BET} associated with the presence of mesopores (S_{meso}) is the lowest (67%). For the rest of the samples, this percentage was in the range 82–93%. The PSD (pore size distribution), obtained by the DFT method, displays the presence of a bimodal micro-mesoporus structure with mesopores of mainly 3.9 nm.

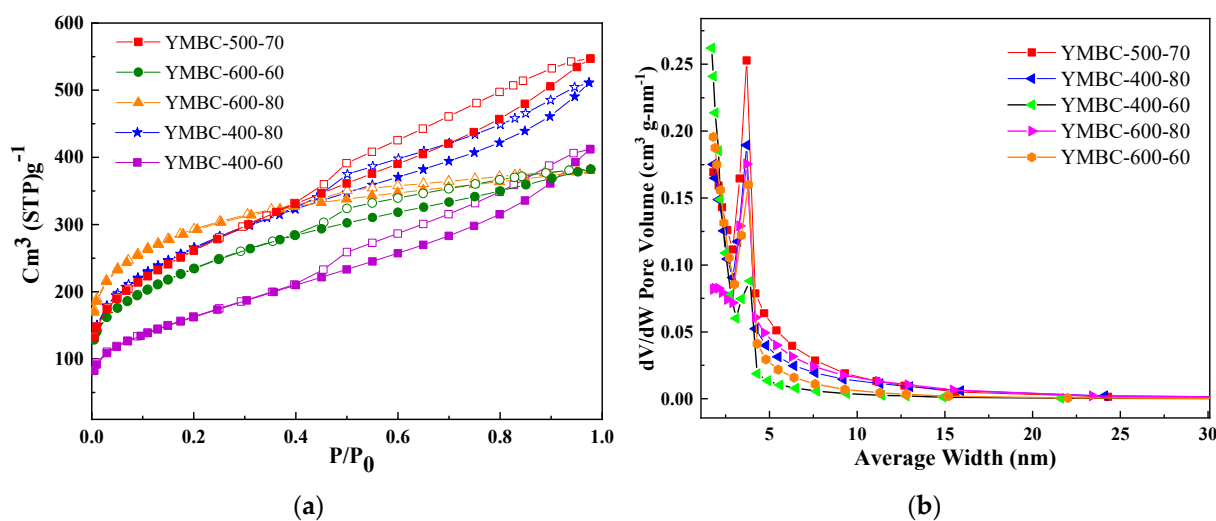


Figure 2. N₂ adsorption (symbol close)–desorption (symbol open) isotherms (a) and PSD (b) of YMBC samples. (Desorption loop symbol open and adsorption loop symbol close).

Figure 3 shows the potentiometric titration with n-butylamine curves of YMBC materials. All the solids display E_i values > 350 mV [32] as a result of the existence of very strong acid sites (see the classification in the Supplementary Materials). The samples carbonized at a lower temperature (YMBC-400-80 and YMBC-400-60 samples) present slightly higher E_i values (416 and 402 mV, respectively) than YMBC-600-80, YMBC-600-60, and YMBC-500-70 samples (377, 389, and 390 mV, respectively) obtained at 600 and 500 °C.

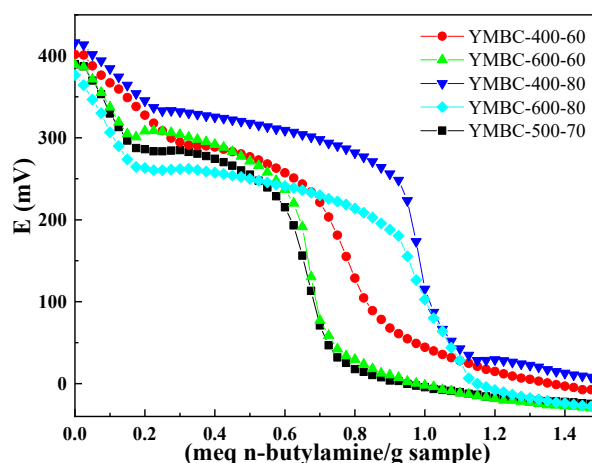
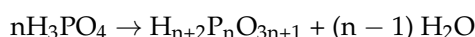


Figure 3. Potentiometric titration with n-butylamine curves of YMBC-X-Z samples.

The area under the potentiometric titration curve provides N_{AS} (the number of acid sites). The samples prepared using a H_3PO_4 :YMT ratio equal to 80 wt% (YMBC-400-80 and YMBC-600-80 samples) present higher N_{AS} values (329 and 288 meq n-butylamine g^{-1} , respectively) than YMBC-400-60 and YMBC-600-60 samples (263 and 243 meq n-butylamine g^{-1} , respectively) obtained employing a H_3PO_4 :YMT ratio equal to 60 wt%. On the other hand, regardless of the H_3PO_4 :YMT ratio used, the N_{AS} values decreased with the increment of the carbonization temperature. The lower N_{AS} value is probably due to the different amounts of organic groups generated during the carbonization at different temperatures and also to the species resulting from the H_3PO_4 thermal treatment.

At low temperatures, H_3PO_4 catalyzes the hydrolysis of glycosidic bonds in hemicellulose and cellulose, and also the cleavage of aryl ether bonds in lignin [33]. According to Yaxin Li et al. [34], the following reactions might occur when the temperature increases from 100 to 400 °C:



The temperature rise to 700 °C could dehydrate the $H_{n+2}P_nO_{3n+1}$ species to P_4O_{10} . This species can behave as an oxidant, react with carbon, and generate new pores and/or widen the existing ones. H_3PO_4 and $H_{n+2}P_nO_{3n+1}$ species might combine with different organic groups present in the lignocellulosic material (i.e., phenolic and carbonyl groups) to form P-O-C linkages, such as phosphate and polyphosphate esters. Additionally, the YMBC has -COOH, -C=O, and -C-OH species that can be protonated in the presence of $H_{n+2}P_nO_{3n+1}$ species [35], allowing the electrostatic interaction of these groups and the anions $[H_{n+2}P_nO_{3n+1}]^{x-}$. According to Rosas et al. [36], the acid species could be removed and collected by a washing procedure. Nevertheless, some of these groups last on the carbon after the washing.

As a result of the washing tests performed using water and n-propanol as solvents, the P content decreases significantly (see Table S2 in the Supplementary Material). For example, the P content of the YMBC-400-80 sample (73 mg g^{-1}) decreases to 43 and 45 mg g^{-1} after 9 h at reflux temperature in water and n-propanol, respectively (YMBC-400-80_W and

YMBC-400-80_{NP} samples). On the other hand, the percentage of the original P content removed was lower for the materials synthesized using a H₃PO₄:YMT ratio equal to 60 wt% (YMBC-400-60 and YMBC-600-60 samples). No significant change in the P content was produced using toluene as a solvent.

The TGA diagram of the YMBC-400-80 sample (Figure 4) shows two small weight loss steps at temperatures below 400 °C. The first one, at temperatures lower than 100 °C (9.7%), is assigned to moisture release and the second, in the range of 100–400 °C (8.6%), to the thermal decomposition of hemicellulose residues [37]. The weight loss (in the 400–600 °C range) at temperatures higher than that used for the thermal treatment of the sample (400 °C) was ascribed to the thermal decomposition of lignin and cellulose residues (39.3%). The FT-IR spectra of the gaseous species released during the thermogravimetric analysis (see Figure S3 in the Supplementary Materials) reveal bands at 1512 cm^{−1} (C=C), 1750 cm^{−1} (C=O), 3020 cm^{−1} (C–H), 3650 cm^{−1} (O–H), 1620 cm^{−1} (C–P), and 660 cm^{−1} (P–O). The presence of carbon–phosphorus species (C–P and P–O bands), methane (from lignin residue decomposition), and phenolic acid compounds (O–H) was detected using TGA-FT-IR during the phosphoric acid-assisted pyrolysis of lignocellulose [38].

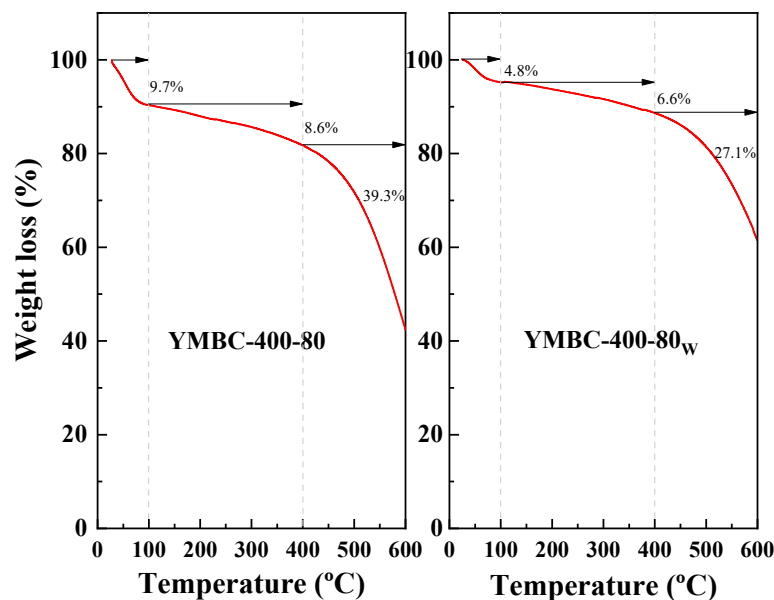


Figure 4. TGA diagram of YMBC-400-80 and YMBC-400-80_W samples.

The TGA diagram of YMBC-400-80_W and YMBC-400-80_{NP} samples (obtained by refluxing YMBC-400-80 with water and n-propanol, respectively) presents the three weight loss steps previously mentioned. However, the weight loss percentage decreased significantly. In the case of YMBC-400-80_W (Figure 4), the estimated percentages were 4.8%, 6.6%, and 27.1%, respectively. FT-IR spectra of gaseous species generated during the TGA analysis reveal the intensity drop of the C–P and P–O bands, mainly due to P elimination during the refluxing tests (Figure S1). As a consequence of YMBC-400-80_W and YMBC-400-80_{NP}'s lower P content, the generation of volatile compounds decreases and the band intensity also drops.

From the potentiometric titration curves of YMBC materials refluxed in n-propanol (Figure 5), we can see that the E_i values remain practically unchanged (YMBC-400-60_{NP} 390, YMBC-400-80_{NP} 401, YMBC-600-60_{NP} 385, YMBC-600-80_{NP} 395, and YMBC-500-70_{NP} 389 mV). However, N_{AS} decreases significantly as a result of the phosphorus species removal (see Table S2 in the Supplementary Materials). The samples prepared using a H₃PO₄:YMT ratio equal to 80 wt% (YMBC-400-80 and YMBC-600-80 samples) undergo the highest reduction in N_{AS} (65 and 53 meq n-butylamine/g sample, respectively). We can also see that the N_{AS} reduction was lower for the samples treated at 600 °C. The

YMBC-500-70 sample was the one least affected by the reflux treatment, its N_{AS} decreased by approximately 23%.

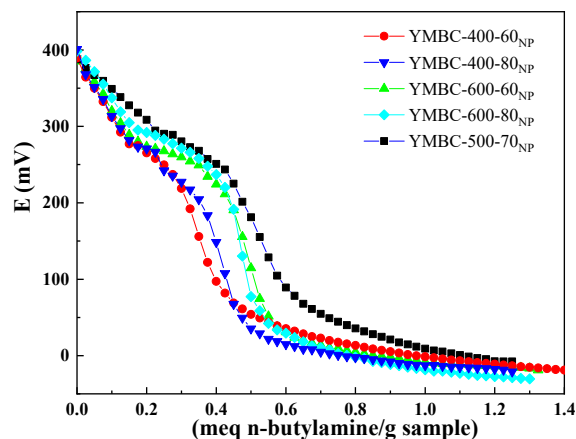


Figure 5. Potentiometric titration with n-butylamine curves of YMBC-X- Z_{NP} samples.

The FT-IR spectra of YMBC-400-80 and YMBC-600-80 samples (Figure 6) display several bands in the region between 2000 and 600 cm^{-1} . The band near 1700 cm^{-1} could be assigned to unconjugated carbonyl/carboxyl stretching [39] and the one around 1580 cm^{-1} could be assigned to aromatic ring or C=C stretching vibrations [34]. The adsorption around 1200 cm^{-1} might be ascribed to O–C stretching vibrations in P–O–C (aromatic) linkage, to the stretching mode of hydrogen-bonded P=O, and to P=OOH [40,41]. Moreover, the adsorption at 985 cm^{-1} could be due to the stretching symmetric vibrations of P–O bond [42].

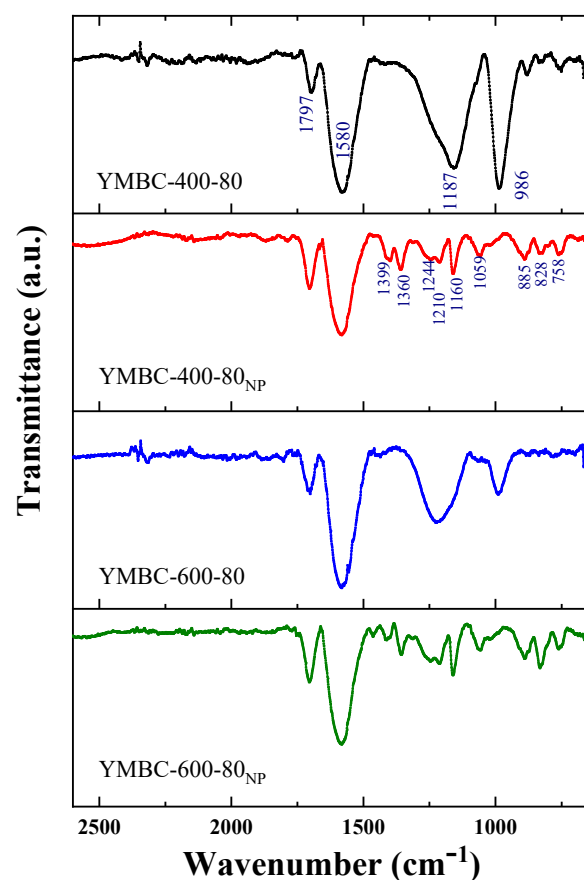


Figure 6. FT-IR spectra of YMBC-400-80, YMBC-400-80 $_{NP}$, YMBC-600-80, and YMBC-600-80 $_{NP}$ samples.

The intensity of these two bands decreases significantly as a result of the reflux treatment (Figure 6) and the leaching of $H_{n+2}P_nO_{3n+1}$ species loosely attached to the carbon surface. We can also see that a new set of low-intensity bands (previously overlapped by the intense bands mentioned before) appears (see the assignment in Table S3 in the Supplementary Materials).

The ^{31}P MAS-NMR spectra of YMBC-400-80 and YMBC-400-80_W samples (Figure 7) show a wide signal with a maximum at -1.5 ppm. In the case of the YMBC-400-80_W spectrum, the lower signal intensity is due to the lower P content of the sample. Their spectral deconvolution shows three signals that can be assigned to the presence of inorganic and organic P species [38]. The most intense signal (centered at -1.6 ppm) is ascribed mainly to ortho- and pyrophosphates. The signals centered at -5.1 and 5.1 ppm could be assigned to phosphate di- and monoesters, respectively [43]. ^{31}P MAS-NMR results reveal that inorganic phosphates (ortho- and pyrophosphates) and phosphate diesters are the main P species present in both samples (42% and 38%, respectively). The reflux treatment with water or n-propanol removes ortho- and pyrophosphate species in a slightly higher percentage than the others. Taking into account the above-mentioned results, we can conclude that the reflux treatment is essential to avoid the possibility of phosphorus species leaching.

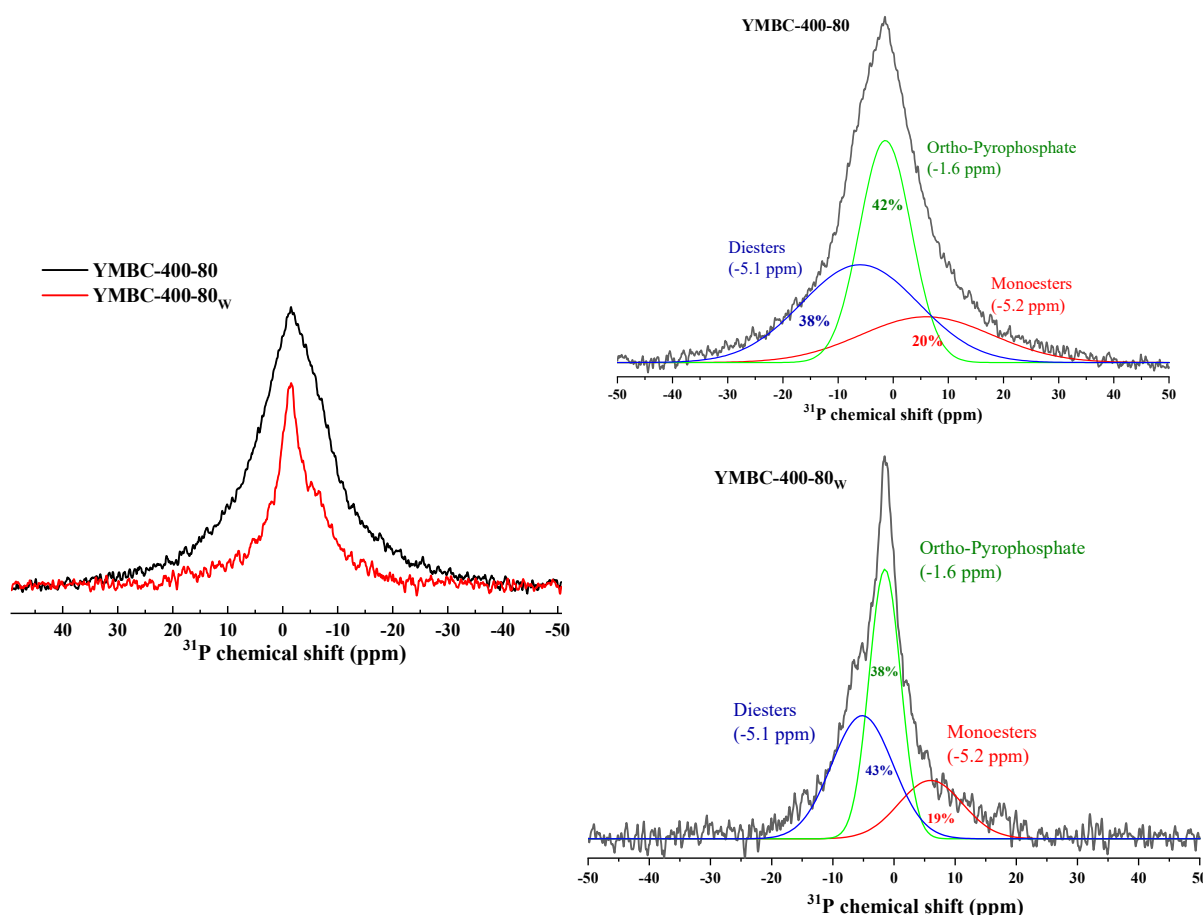
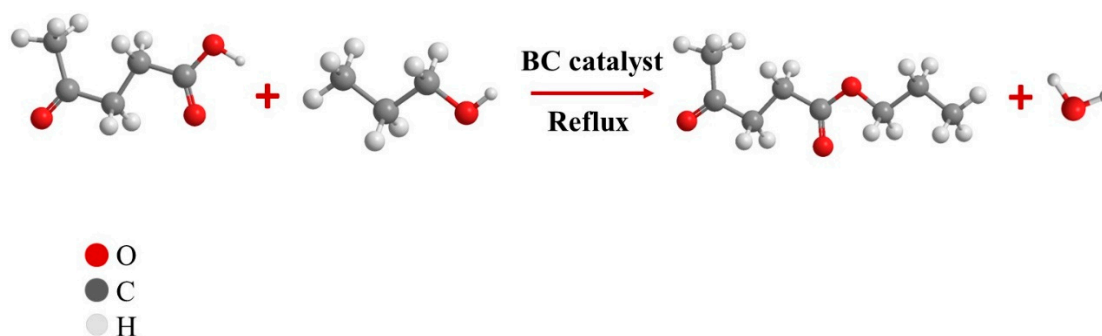


Figure 7. ^{31}P MAS-NMR spectra and deconvoluted P species of YMBC-400-80 and YMBC-400-80_W samples.

So, the catalytic properties of YMBC-400-60_{NP}, YMBC-400-80_{NP}, YMBC-600-60_{NP}, YMBC-600-80_{NP}, and YMBC-500-70_{NP} samples were first evaluated in the esterification of levulinic acid with n-propanol (Scheme 1).



Scheme 1. Model esterification of levulinic acid with n-propanol.

Initially, a noncatalytic reaction using levulinic acid (2 mmol) and n-propanol (2 mL) was performed. Under the experimental conditions tested (97 °C, 9 h), a very low conversion of levulinic acid (<5%) was obtained. The levulinic acid conversion increased significantly when YMBC-X-Y_{NP} materials were used as catalysts (Table 4). Under these experimental conditions, no side products were detected.

Table 4. Effect of different synthesized catalysts on n-propyl levulinate yield.

Entry	Catalyst	Fresh	1st Reuse	2nd Reuse	3rd Reuse
1	YMBC-400-60 _{NP}	27	-	-	-
2	YMBC-400-80 _{NP}	25	-	-	-
3	YMBC-600-60 _{NP}	47	48	46	-
4	YMBC-600-80 _{NP}	41	40	43	-
5	YMBC-500-70 _{NP}	49	49	48	47

Reaction conditions: levulinic acid (2 mmol); n-propanol (2 mL); catalyst (80 mg); temperature, 97 °C; time, 9 h; stirring rate, 600 rpm.

The n-propyl levulinate yields obtained using YMBC-400-60_{NP}, YMBC-400-80_{NP} materials as catalysts were significantly lower than those achieved employing YMBC-600-60_{NP}, YMBC-600-80_{NP}, and YMBC-500-70_{NP} catalysts.

This agreed with the fact that YMBC-400-60_{NP} and YMBC-400-80_{NP} acidic properties (E_i and N_{AS} values) were lower than those of the other three catalysts. The reusability of the YMBC-600-60_{NP}, YMBC-600-80_{NP}, and YMBC-500-70_{NP} catalysts (those with the highest catalytic performance) was evaluated. At the end of each run, the solid was separated, washed with n-propanol, dried at 40 °C in vacuum, and then reused. The n-propyl levulinate yields obtained after reusing the catalysts several times were similar to those achieved using the fresh ones.

Additional experiments were carried out using the YMBC500-70_{NP} catalyst to verify the absence of diffusional problems in the system. The material was ground (size particle lower than 0.149 mm) and evaluated using two different agitation speeds (800 and 200 rpm). The n-propyl levulinate yields obtained for the ground and unground material using 800 rpm (51% and 49%, respectively) were similar to the yield obtained at 600 rpm (49%) using the unground YMBC500-70_{NP} catalyst (particle size ~1.41 mm). The yields obtained using 200 rpm were slightly lower (47% and 44% for the ground and unground catalysts, respectively). So, we can conclude that there are no diffusion restrictions under the reaction conditions used to evaluate the materials.

Table 5 shows the YMBC500-70_{NP} catalytic activity under different reaction conditions: reaction time, temperature, and catalyst amount. The n-propyl levulinate yields increased significantly with the reaction time increment from 6 to 24 h (Table 5, entries 1–3). Only a marginal yield increment was achieved (from 88% to 96%, Table 5, entries 3 and 4) when the reaction time was raised from 24 to 48 h.

Table 5. Effect of different reaction conditions on levulinic acid esterification reaction with n-propanol, using YMBC-500-70 previously washed.

Entry	Time (h)	Temp. (°C)	Catalyst Amount (mg)	Yield (%)
1	6	97	80	49
2	12	97	80	57
3	24	97	80	88
4	48	97	80	94
5	6	77	80	20
6	6	87	80	28
7	6	97	40	37
8	6	97	120	53

Reaction conditions: levulinic acid (2 mmol); n-propanol (2 mL); catalyst: YMBC-500-70NP; stirring rate: 600 rpm.

As we can see (Table 5, entries 5 and 6), the n-propyl levulinate yields obtained using lower temperatures (77 and 87 °C, respectively) dropped remarkably. So, the analysis of the catalyst amount effect was conducted at 97 °C.

Table 5 (entries 1, 7, and 8) displays the effect of YMBC5-70_{NP} amount on the yield of n-propyl levulinate. The yields of n-propyl levulinate increased from 37% to 49% when the amount of YMBC5-70% rose from 40 to 80 mg. However, no significant yield changes (53%) were observed with further increments in the catalyst amount (120 mg).

Using the best reaction conditions found for the synthesis of n-propyl levulinate, a series of experiments were carried out using different alcohols to study the effect of alcohol nature on the levulinic ester yield.

No significant differences in the ester yields (Table 6, entries 1–3) were observed for primary alcohols (n-propanol, 49%; n-butanol, 49%; and n-pentanol, 47%). However, the esters formed by branched alcohols (isopropanol and isobutanol) were obtained with slightly lower reaction yields. In the case of t-butanol (a tertiary alcohol that is sterically hindered) and phenol, a very low-nucleophilicity substrate, the reaction did not lead to the respective ester.

Table 6. Effect of alcohol nature on the levulinic ester yield using YMBC-500-70 previously washed.

Entry	Alcohol	Yield (%)
1	n-Propanol	49
2	n-Butanol	49
3	n-Pentanol	47
4	i-Propanol	39
5	i-Butanol	45
6	t-Butanol	-
7	Phenol	-

Reaction conditions: levulinic acid (2 mmol); alcohol (2 mL); catalyst: YMBC-500-70_{NP} (80 mg); temperature, 97 °C; time, 6 h; stirring rate: 600 rpm.

The FT-IR spectrum and potentiometric titration curve of the YMBC-500-70_{NP} spent catalyst were obtained. No significant differences between the FT-IR spectra of the spent and fresh sample were detected. The main characteristics of the potentiometric titration curves of used YMBC-500-70_{NP} were also quite similar to those of the fresh sample.

3. Experimental Methods

3.1. General Remarks

Before their use, all the reagents (analytical grade) employed for the esterification of itaconic were purified (by recrystallization or distillation). The reactions were followed using standard procedures, TLC and GC-MS. In addition, for each reaction the yields were calculated. The identification of pure products was carried out by comparison with authentic samples prepared by a classical procedure brief in the literature for esterification

reactions. The reaction progress was followed using a Shimadzu (Kyoto, Japan, model 2014 with a FID detector) gas chromatograph and the products were identified by GC–MS using an HP 5971 attached to an HP GC. The detailed operation conditions can be seen in the Supplementary Materials.

3.2. Factorial Experimental Design 2^k

The response surface method (RSM) of factorial 2^2 design-type by means of the Statgraphics Centurion XVI software (version 19.4.04) was employed to model and analyze the optimized activated carbon synthesis conditions. Two factorial points (X_1 : H_3PO_4 :YMT ratios, wt% and X_2 : carbonization temperature, °C) in a two-level factorial design ($k = 2$) were taken as the design variables, and the development of the specific surface area (S_{BET} : $m^2 g^{-1}$) from yerba mate twigs was used as the response value. The experimental runs are shown in Table 1. The carbonization temperature ranges and concentration of activating agent (H_3PO_4 , NaOH) were 300–600 °C and 20–80%, respectively.

3.3. Yerba Mate Activated Carbon Preparation

The activated carbon synthesis was carried out basically following the procedure previously reported [26,37], using yerba mate (*I. paraguayensis*) supplied by a local manufacturer (HReñuk S.A. Argentina, Apóstoles, Argentina) as a precursor. The twigs were separated from the leaves, milled, and then sieved to obtain particles with sizes in the range of 2–3 mm. They were cleaned with deionized water to eliminate impurities and dust on the surface and then dried at 100 °C for 12 h to remove moisture. The resulting samples were labeled as YMT. Afterwards, YMT samples were impregnated with activating agent solutions (H_3PO_4 85 wt%, Anedra®, Buenos Aires, Argentina) and heated at 75 °C for 1 h with constant stirring at 350 rpm. The H_3PO_4 concentration was fixed to obtain H_3PO_4 :YMT ratios between 60 and 80 wt%. Then, the slurries were filtered and the solid part dried at 80 °C for 10 h. Finally, the solids were carbonized at temperatures in the range between 400 and 600 °C for 1 h (5 °C min^{-1} heating rate) under a N_2 atmosphere using an electric furnace (Estigia®, Buenos Aires, Argentina). The samples were named YMBC-X-Z (where X: H_3PO_4 :YMT ratios, wt% and Z: carbonization temperature, °C).

The solids were cooled under a N_2 flow, and then washed with distilled hot water until the effluent pH was ~6.5. Finally, the resulting YMBC-X-Z materials were dried for 24 h at 100 °C and then stored in a desiccator. Additional washing tests were performed using n-propanol and toluene as solvents. To perform these tests, 500 mg of YMBC-X-Z materials and 10 mL of solvent were stirred for 9 h at reflux temperature. The solids were separated by filtration, dried at 100 °C for 24 h, and then kept in a desiccator.

3.4. Physicochemical Characterization

The S_{BET} (specific surface area) and D_p (mean pore size) of the solids were estimated from the adsorption–desorption isotherms of N_2 at -196 °C, using an ASAP 2020 equipment, Norcross, GA, USA, and degasification for 1 h at 100 °C. The morphology was studied by scanning electron microscopy (SEM, Phillips 505, Eindhoven, The Netherlands) with an energy-dispersive X-ray EDAX 9100 analyzer. The chemical species in the materials were evaluated by FT-IR (Fourier transform infrared spectroscopy) Perkin-Elmer (Waltham, MA, USA), ^{31}P MAS-NMR (^{31}P magic-angle spinning–nuclear magnetic resonance) Bruker Avance II equipment, (Coventry, UK), and TGA-FTIR, TA Instruments Q 50 equipment, (Elstree, UK), experiments (see the equipment and conditions used in the Supplementary Materials). Finally, the acidic characteristics of the YMBC materials were evaluated whilst titrating with an n-butylamine solution in acetonitrile by the solid suspending in the acetonitrile (Metrohm 794 Basic Titrino apparatus, Herisau, Switzerland). In order to determine the P content in the solids, a portion of the YMBC-X-Z materials was disaggregated (SM 3030G). The P content in the resulting solutions was measured by atomic absorption spectrometry (SM 3110) using a 240 Varian AA spectrophotometer (Ottawa, ON, Canada).

3.5. Catalytic Test

Esterification reactions were carried out in a Pyrex stirred batch reactor at 67–97 °C. The reactor was loaded with 2 mL of n-propanol, 2 mmol of levulinic acid, and a chosen amount of the catalyst (YMBC-X-Z). TLC was used to follow the esterification until a reaction time of 24 h, using mixtures of ethylacetate/hexane as a solvent. TLC aluminum sheets (silica gel 60 F254 Merck, Rahway, NJ, USA) were used.

The catalyst was separated by filtration (Boeco, Hamburg, Germany, FTR 3.102.110 filter paper) or centrifugation (2000 rpm), where it was very finely divided, and then washed twice with 2 mL n-propanol. The washing liquids and filtrate were put together and concentrated in vacuum. CH_2Cl_2 (10 mL) was used to dissolve the residue. The solution obtained was washed with NaHCO_3 5% (3×2 mL) and water (1×5 mL) to separate the unreacted levulinic acid. Anhydrous Na_2SO_4 was used to dry the organic phase, and the solvent was evaporated to afford crude n-propyl levulinate. The product was identified by comparing its mass spectrum with the one of an n-propyl levulinate sample prepared according to Barberot et al. [44]. The reaction yield was expressed as the ratio of % moles of product to moles of initial substrate.

3.6. Catalytic Reuse

At the end of each test, the YMBC-X-Z was separated from the reaction mixture by filtration, washed twice with 2 mL of n-propanol, dried under vacuum at room temperature (25 °C) for 24 h, and then reused in two successive reaction cycles.

3.7. Mass Spectrum of Synthesized Alkyl Levulinates

n-Propyl levulinate: m/z : 158 (1%), 143 (5%), 116 (7%), 99 (63%), 74 (30%), 55 (4%), 43 (100%), 29 (3%).

Isopropyl levulinate: m/z : 143 (3%), 130 (2%), 116 (8%), 99 (64%), 74 (23%), 56 (16%), 43 (10%).

n-Butyl levulinate: m/z : 172 (1%), 157 (8%), 133 (10%), 117 (20%), 99 (100%), 74 (60%), 56 (25%), 43 (78%), 29 (18%).

Isobutyl levulinate: m/z : 172 (<1%), 157 (1%), 130 (5%), 117 (10%), 99 (70%), 74 (31%), 57 (62%), 56 (40%), 43 (100%), 41 (33%), 29 (25%).

n-Pentyl levulinate: m/z : 186 (<1%), 172 (<1%), 143 (1%), 130 (3%), 115 (5%), 103 (81%), 85 (100%), 70 (91%), 57 (90%), 55 (61%), 43 (70%), 41 (75%), 29 (62%).

4. Conclusions

A series of acid catalysts named YMBC-400-60, YMBC-400-80, YMBC-600-60, YMBC-600-80, and YMBC-500-70 were prepared by chemical (H_3PO_4) and thermal activation of yerba mate twigs. The optimal experimental conditions (H_3PO_4 concentration and carbonization temperature) to obtain activated carbon from yerba mate twigs with suitable textural and acidic properties to be used as heterogeneous catalysts were identified using an experimental design methodology of central composite design (CCD). The results showed that the YMBC with the highest S_{BET} value ($1031 \text{ m}^2 \text{ g}^{-1}$), mainly because of the existence of mesopores ($S_{\text{meso}}/S_{\text{BET}} = 66\%$), was the YMBC-600-80 sample, activated with the highest H_3PO_4 :YMT ratio and carbonization temperature (80% and 600 °C, respectively). However, the YMBC-500-70 material displayed a high specific surface area ($S_{\text{BET}} = 864 \text{ m}^2 \text{ g}^{-1}$) and the highest $S_{\text{meso}}/S_{\text{BET}}$ contribution (82%).

The YMBC-X-Z materials showed acid sites with $E_i > 350$ mV (very strong), whose number increased with the increment of H_3PO_4 :YMT ratio used during their synthesis.

FT-IR and ^{31}P MAS-NMR characterization showed that $\text{H}_{n+2}\text{P}_n\text{O}_{3n+1}$ species loosely attached to the carbon surface were successfully removed by the reflux treatment with n-propanol or water. These treatments are essential to avoid the possibility of phosphorus species leaching when the materials are used as heterogeneous catalysts in the synthesis of levulinic acid esters. The highest n-propyl levulinate yields were achieved employing YMBC-600-60_{NP}, YMBC-600-80_{NP}, and YMBC-500-70_{NP} catalysts, materials that present re-

markable acidic properties (higher E_i and N_{AS} values) and were reused in four consecutive reaction cycles, showing excellent results in the formation of levulinic acid esters.

The reusability of YMBC-600-60_{NP}, YMBC-600-80_{NP}, and YMBC-500-70_{NP} catalysts (those with the highest catalytic performance) was evaluated. It can be concluded that YMBC-600-60_{NP}, YMBC-600-80_{NP}, and YMBC-500-70_{NP} catalysts were active and led to very good yields. So, they can be considered as appropriate candidates to replace the mineral acids currently used for levulinate ester synthesis.

Supplementary Materials: The following supporting information can be downloaded at: <https://www.mdpi.com/article/10.3390/catal14080522/s1>: Figure S1. Micrographic SEM for YMBC-500-70, Figure S2. XRD patterns for YMBC-500-70, Figure S3. FT-IR spectra of the gaseous species released during the thermogravimetric analysis: a. YMBC-500-70, and b. YMBC-500-70_{NP}; Table S1. The solid catalysts listed in literature for the esterification of levulinic acid with ethanol, Table S2. P content and acidic properties of YMBC samples; Table S3. FT-IR band assignments. References [45–51] are cited in the Supplementary Materials.

Author Contributions: J.J.A.-D.: methodology, investigation, data curation, formal analysis, writing—original draft. A.S.: methodology, investigation, formal analysis. G.A.P.: methodology, investigation, formal analysis. D.M.R.: methodology, investigation, formal analysis. J.A.R.-H.: supervision, data curation, formal analysis. G.P.R.: conceptualization, methodology, supervision, data curation, formal analysis, writing—original draft, funding acquisition, project administration. L.R.P.: conceptualization, methodology, supervision, formal analysis, writing—review and editing, funding acquisition, project administration. All authors have read and agreed to the published version of the manuscript.

Funding: This research received funding from “Consejo Nacional de Investigaciones Científicas y Técnicas”-CONICET Argentina for the economic support (grant PIP 1492) and UNLP (grant X 879).

Data Availability Statement: Data are contained within the article and Supplementary Materials.

Conflicts of Interest: The authors declare no conflicts of interest.

References

- Shan, J.; Wang, Q.; Hao, H.; Guo, H. Critical Review on the Synthesis of Levulinate Esters from Biomass-Based Feedstocks and Their Application. *Ind. Eng. Chem. Res.* **2023**, *62*, 17135–17147. [\[CrossRef\]](#)
- Liu, R.; Guo, Y.; Pei, M.; Chen, Y.; Zhang, L.; Li, L.; Chen, Q.; Tian, Y.; Xie, H. Cellulose Levulinate Ester as a Robust Building Block for the Synthesis of Fully Biobased Functional Cellulose Esters. *Int. J. Biol. Macromol.* **2023**, *246*, 125654. [\[CrossRef\]](#)
- Pasquale, G.; Vázquez, P.; Romanelli, G.; Baronetti, G. Catalytic Upgrading of Levulinic Acid to Ethyl Levulinate Using Reusable Silica-Included Wells-Dawson Heteropolyacid as Catalyst. *Catal. Commun.* **2012**, *18*, 115–120. [\[CrossRef\]](#)
- Zhao, H.; Jia, Y.; Liang, X.; Hao, J.; Xu, G.; Chen, B.; He, C.; Jiao, Y.; Chang, C. Theoretical and Experimental Study of 5-Ethoxymethylfurfural and Ethyl Levulinate Production from Cellulose. *Chem. Eng. J.* **2024**, *480*, 148093. [\[CrossRef\]](#)
- Hassan, A.H.; Zainol, M.M.; Samion, M.A.; Azlan, M.A.; Asmadi, M.; Mohamad Daud, A.R.; Saad, I.; Mohd Nor Azman, N.A.N. Synthesis of Ethyl Levulinate over Sulfonated Lignin-Based Carbon Catalyst as a Fuel Additive to Biodiesel-Diesel Blends towards Engine Emissions. *J. Clean. Prod.* **2023**, *418*, 138101. [\[CrossRef\]](#)
- Lei, T.; Wang, Z.; Li, Y.; Li, Z.; He, X.; Zhu, J. Performance of a Diesel Engine with Ethyl Levulinate-Diesel Blends: A Study Using Grey Relational Analysis. *Bioresources* **2013**, *8*, 2696–2707. [\[CrossRef\]](#)
- Unlu, D.; Ilgen, O.; Hilmioglu, N.D. Biodiesel Additive Ethyl Levulinate Synthesis by Catalytic Membrane: SO₄²⁻/ZrO₂ Loaded Hydroxyethyl Cellulose. *Chem. Eng. J.* **2016**, *302*, 260–268. [\[CrossRef\]](#)
- Badgujar, K.C.; Badgujar, V.C.; Bhanage, B.M. A Review on Catalytic Synthesis of Energy Rich Fuel Additive Levulinate Compounds from Biomass Derived Levulinic Acid. *Fuel Process. Technol.* **2020**, *197*, 106213. [\[CrossRef\]](#)
- Gómez Millán, G.; Hellsten, S.; Llorca, J.; Luque, R.; Sixta, H.; Balu, A.M. Recent Advances in the Catalytic Production of Platform Chemicals from Holocellulosic Biomass. *ChemCatChem* **2019**, *11*, 2022–2042. [\[CrossRef\]](#)
- Ogino, I.; Suzuki, Y.; Mukai, S.R. Esterification of Levulinic Acid with Ethanol Catalyzed by Sulfonated Carbon Catalysts: Promotional Effects of Additional Functional Groups. *Catal. Today* **2018**, *314*, 62–69. [\[CrossRef\]](#)
- Popova, M.; Shestakova, P.; Lazarova, H.; Dimitrov, M.; Kovacheva, D.; Szegedi, A.; Mali, G.; Dasireddy, V.; Likozar, B.; Wilde, N.; et al. Efficient Solid Acid Catalysts Based on Sulfated Tin Oxides for Liquid Phase Esterification of Levulinic Acid with Ethanol. *Appl. Catal. A Gen.* **2018**, *560*, 119–131. [\[CrossRef\]](#)
- Kothe, V.; Melfi, D.T.; dos Santos, K.C.; Corazza, M.L.; Ramos, L.P. Thermodynamic Analysis, Experimental and Kinetic Modeling of Levulinic Acid Esterification with Ethanol at Supercritical Conditions. *Fuel* **2020**, *260*. [\[CrossRef\]](#)

13. Russo, V.; Tesser, R.; Rossano, C.; Coglianò, T.; Vitiello, R.; Leveneur, S.; Di Serio, M. Kinetic Study of Amberlite IR120 Catalyzed Acid Esterification of Levulinic Acid with Ethanol: From Batch to Continuous Operation. *Chem. Eng. J.* **2020**, *401*, 126126. [\[CrossRef\]](#)
14. Mthembu, L.D.; Lokhat, D.; Deenadayalu, N. Esterification of Levulinic Acid to Ethyl Levulinate: Optimization of Process Conditions Using Commercial Levulinic Acid and Extension to the Use of Levulinic Acid Derived from Depithed Sugarcane Bagasse. *Biomass Convers. Biorefin.* **2023**, *13*, 3113–3122. [\[CrossRef\]](#)
15. Sahu, P.; Sakthivel, A. Zeolite- β Based Molecular Sieves: A Potential Catalyst for Esterification of Biomass Derived Model Compound Levulinic Acid. *Mater. Sci. Energy Technol.* **2021**, *4*, 307–316. [\[CrossRef\]](#)
16. Badia, J.H.; Ramírez, E.; Soto, R.; Bringué, R.; Tejero, J.; Cunill, F. Optimization and Green Metrics Analysis of the Liquid-Phase Synthesis of Sec-Butyl Levulinate by Esterification of Levulinic Acid with 1-Butene over Ion-Exchange Resins. *Fuel Process. Technol.* **2021**, *220*. [\[CrossRef\]](#)
17. Ristiana, D.D.; Suyanta, S.; Nuryono, N. Sulfonic Acid-Functionalized Silica with Controlled Hydrophobicity as an Effective Catalyst for Esterification of Levulinic Acid. *Mater. Today Commun.* **2022**, *32*, 103953. [\[CrossRef\]](#)
18. Bakhtiari, B.; Najafi Chermahini, A.; Babaei, Z. Design of an Acidic Sulfonated Mesoporous Carbon Catalyst for the Synthesis of Butyl Levulinate from Levulinic Acid. *Environ. Prog. Sustain. Energy* **2021**, *40*, 1–13. [\[CrossRef\]](#)
19. Veluturla, S.; Kottam, N.; Vandana, P.; Shetty, A.; Shankar, V. Process Optimisation and Kinetic Study for Esterification of Levulinic Acid and N-Butanol Using Sulfonated Titania–Zirconia Heterogeneous Catalyst. *J. Chem. Technol. Biotechnol.* **2024**, *99*, 626–636. [\[CrossRef\]](#)
20. Démolis, A.; Essayem, N.; Rataboul, F. Synthesis and Applications of Alkyl Levulinates. *ACS Sustain. Chem. Eng.* **2014**, *2*, 1338–1352. [\[CrossRef\]](#)
21. Nelson Appaturi, J.; Andas, J.; Ma, Y.K.; Lee Phoon, B.; Muazu Batagarawa, S.; Khoerunnisa, F.; Hazwan Hussin, M.; Ng, E.P. Recent Advances in Heterogeneous Catalysts for the Synthesis of Alkyl Levulinate Biofuel Additives from Renewable Levulinic Acid: A Comprehensive Review. *Fuel* **2022**, *323*, 124362. [\[CrossRef\]](#)
22. Hassan, A.H.; Zainol, M.M.; Zainuddin, K.R.; Rosmadi, H.A.; Asmadi, M.; Rahman, N.A.; Amin, N.A.S. A Review on Alkyl Levulinates Synthesis from Renewable Levulinic Acid Using Various Modified Carbon-Based Catalysts. *Malays. J. Chem.* **2022**, *24*, 264–282. [\[CrossRef\]](#)
23. Yan, L.; Yao, Q.; Fu, Y. Conversion of Levulinic Acid and Alkyl Levulinates into Biofuels and High-Value Chemicals. *Green. Chem.* **2017**, *19*, 5527–5547. [\[CrossRef\]](#)
24. Liu, X.; Yang, W.; Zhang, Q.; Li, C.; Wu, H. Current Approaches to Alkyl Levulinates via Efficient Valorization of Biomass Derivatives. *Front. Chem.* **2020**, *8*, 1–13. [\[CrossRef\]](#) [\[PubMed\]](#)
25. Budarin, V.; Luque, R.; Macquarrie, D.J.; Clark, J.H. Towards a Bio-Based Industry: Benign Catalytic Esterifications of Succinic Acid in the Presence of Water. *Chem. A Eur. J.* **2007**, *13*, 6914–6919. [\[CrossRef\]](#)
26. Alvear-Daza, J.J.; Pasquale, G.A.; Rengifo-Herrera, J.A.; Romanelli, G.P.; Pizzio, L.R. Mesoporous Activated Carbon from Sunflower Shells Modified with Sulfonic Acid Groups as Solid Acid Catalyst for Itaconic Acid Esterification. *Catal. Today* **2021**, *372*, 51–58. [\[CrossRef\]](#)
27. Urruchua, F.C.; Fernández, M.A.; Jaworski, M.; Mendoza Zelis, P.; Olivelli, M.S.; Montes, M.L. Yerba Mate Waste: Transformation to Magnetic Composites for the Adsorption of Chemically Diverse Pollutants. *J. Environ. Chem. Eng.* **2023**, *11*, 110824. [\[CrossRef\]](#)
28. Jerez, F.; Ramos, P.B.; Córdoba, V.E.; Ponce, M.F.; Acosta, G.G.; Bavio, M.A. Yerba Mate: From Waste to Activated Carbon for Supercapacitors. *J. Environ. Manag.* **2023**, *330*, 117158. [\[CrossRef\]](#) [\[PubMed\]](#)
29. Gomez-Delgado, E.; Nunell, G.; Cukierman, A.L.; Bonelli, P. Agroindustrial Waste Conversion into Ultramicroporous Activated Carbons for Greenhouse Gases Adsorption-Based Processes. *Bioresour. Technol. Rep.* **2022**, *18*, 101008. [\[CrossRef\]](#)
30. Mohan, D.; Abhishek, K.; Sarswat, A.; Patel, M.; Singh, P.; Pittman, C.U. Biochar Production and Applications in Soil Fertility and Carbon Sequestration—a Sustainable Solution to Crop-Residue Burning in India. *RSC Adv.* **2018**, *8*, 508–520. [\[CrossRef\]](#)
31. Sing, K.S.W. Reporting Physisorption Data for Gas/Solid Systems with Special Reference to the Determination of Surface Area and Porosity (Provisional). *Pure Appl. Chem.* **1982**, *54*, 2201–2218. [\[CrossRef\]](#)
32. Chimienti, M.E.; Pizzio, L.R.; Cáceres, C.V.; Blanco, M.N. Tungstophosphoric and Tungstosilicic Acids on Carbon as Acidic Catalysts. *Appl. Catal. A Gen.* **2001**, *208*, 7–19. [\[CrossRef\]](#)
33. Hosseinzadeh, B.; Hadianfard, M.J.; Ruiz-Rosas, R.; Rosas, J.M.; Rodríguez-Mirasol, J.; Cordero, T. Effect of Heating Rate and H₃PO₄ as Catalyst on the Pyrolysis of Agricultural Residues. *J. Anal. Appl. Pyrolysis* **2022**, *168*, 105724. [\[CrossRef\]](#)
34. Li, Y.; Zhang, X.; Yang, R.; Li, G.; Hu, C. The Role of H₃PO₄ in the Preparation of Activated Carbon from NaOH-Treated Rice Husk Residue. *RSC Adv.* **2015**, *5*, 32626–32636. [\[CrossRef\]](#)
35. Abotsi, G.M.K.; Scaroni, A.W. Reaction of Carbons with Ammonia: Effects on the Surface Charge and Molybdenum Adsorption. *Carbon* **1990**, *28*, 79–84. [\[CrossRef\]](#)
36. Rosas, J.M.; Ruiz-Rosas, R.; Rodríguez-Mirasol, J.; Cordero, T. Kinetic Study of the Oxidation Resistance of Phosphorus-Containing Activated Carbons. *Carbon* **2012**, *50*, 1523–1537. [\[CrossRef\]](#)
37. Alvear-Daza, J.J.; Cánneva, A.; Donadelli, J.A.; Manrique-Holguín, M.; Rengifo-Herrera, J.A.; Pizzio, L.R. Removal of Diclofenac and Ibuprofen on Mesoporous Activated Carbon from Agro-Industrial Wastes Prepared by Optimized Synthesis Employing a Central Composite Design. *Biomass Convers. Biorefin.* **2023**, *13*, 13197–13219. [\[CrossRef\]](#)

38. Chu, G.; Wang, W.; Zhao, J.; Zhou, D. Transformation of Phosphorus Species during Phosphoric Acid-Assisted Pyrolysis of Lignocellulose. *Sci. Total Environ.* **2023**, *866*, 161010. [[CrossRef](#)] [[PubMed](#)]
39. Moulefera, I.; García-Mateos, F.J.; Benyoucef, A.; Rosas, J.M.; Rodríguez-Mirasol, J.; Cordero, T. Effect of Co-Solution of Carbon Precursor and Activating Agent on the Textural Properties of Highly Porous Activated Carbon Obtained by Chemical Activation of Lignin With H_3PO_4 . *Front. Mater.* **2020**, *7*, 1–14. [[CrossRef](#)]
40. Puziy, A.M.; Poddubnaya, O.I.; Martínez-Alonso, A.; Suárez-García, F.; Tascón, J.M.D. Synthetic Carbons Activated with Phosphoric—Acid II. Porous Structure. *Carbon* **2002**, *40*, 1507–1519. [[CrossRef](#)]
41. Kumar, A.; Jena, H.M. Preparation and Characterization of High Surface Area Activated Carbon from Fox Nut (*Euryale Ferox*) Shell by Chemical Activation with H_3PO_4 . *Results Phys.* **2016**, *6*, 651–658. [[CrossRef](#)]
42. Jastrzbski, W.; Sitarz, M.; Rokita, M.; Bulat, K. Infrared Spectroscopy of Different Phosphates Structures. *Spectrochim. Acta A Mol. Biomol. Spectrosc.* **2011**, *79*, 722–727. [[CrossRef](#)]
43. Sannigrahi, P.; Ingall, E. Polyphosphates as a Source of Enhanced P Fluxes in Marine Sediments Overlain by Anoxic Waters: Evidence from ^{31}P NMR. *Geochem. Trans.* **2005**, *6*, 52–59. [[CrossRef](#)] [[PubMed](#)]
44. Barberot, C.; Moniot, A.; Allart-Simon, I.; Malleret, L.; Yegorova, T.; Laronze-Cochard, M.; Bentaher, A.; Médebielle, M.; Bouillon, J.P.; Hénon, E.; et al. Synthesis and Biological Evaluation of Pyridazinone Derivatives as Potential Anti-Inflammatory Agents. *Eur. J. Med. Chem.* **2018**, *146*, 139–146. [[CrossRef](#)]
45. Pithadia, D.; Patel, A. Anchored Silicotungstic Acid: Study of the Synthesis of Biofuel Additive from Levulinic Acid & Effect of Supports. *Catal. Today* **2024**, *433*, 114666. [[CrossRef](#)]
46. Tian, Y.; Zhang, R.; Zhao, W.; Wen, S.; Xiang, Y.; Liu, X. A New Sulfonic Acid-Functionalized Organic Polymer Catalyst for the Synthesis of Biomass-Derived Alkyl Levulinates. *Catal. Lett.* **2020**, *150*, 3553–3560. [[CrossRef](#)]
47. Manikandan, K.; Cheralathan, K.K. Heteropoly Acid Supported on Silicalite-1 Possessing Intracrystalline Nanovoids Prepared Using Biomass—An Efficient and Recyclable Catalyst for Esterification of Levulinic Acid. *Appl. Catal. A Gen.* **2017**, *547*, 237–247. [[CrossRef](#)]
48. Enumula, S.S.; Gurram, V.R.B.; Chada, R.R.; Burri, D.R.; Kamaraju, S.R.R. *Clean Synthesis of Alkyl Levulinates from Levulinic Acid over One Pot Synthesized WO_3 -SBA-16 Catalyst*; Elsevier B.V.: Amsterdam, The Netherlands, 2017; Volume 426, ISBN 9140271609.
49. Budarin, V.L.; Clark, J.H.; Henschen, J.; Farmer, T.J.; Macquarrie, D.J.; Mascal, M.; Nagaraja, G.K.; Petchey, T.H.M. Processed Lignin as a Byproduct of the Generation of 5-(Chloromethyl)Furfural from Biomass: A Promising New Mesoporous Material. *ChemSusChem* **2015**, *8*, 4172–4179. [[CrossRef](#)] [[PubMed](#)]
50. Zhang, X.L.; Li, N.; Qin, Z.; Zheng, X.C. Sulfonated Porous Biomass-Derived Carbon with Superior Recyclability for Synthesizing Ethyl Levulinate Biofuel. *Res. Chem. Intermed.* **2020**, *46*, 5325–5343. [[CrossRef](#)]
51. Klähn, M.; Mathias, G.; Kötting, C.; Nonella, M.; Schlitter, J.; Gerwert, K.; Tavan, P. IR Spectra of Phosphate Ions in Aqueous Solution: Predictions of a DFT/MM Approach Compared with Observations. *J. Phys. Chem. A* **2004**, *108*, 6186–6194. [[CrossRef](#)]

Disclaimer/Publisher’s Note: The statements, opinions and data contained in all publications are solely those of the individual author(s) and contributor(s) and not of MDPI and/or the editor(s). MDPI and/or the editor(s) disclaim responsibility for any injury to people or property resulting from any ideas, methods, instructions or products referred to in the content.